Identifying and counting point defects in carbon nanotubes

YUWEI FAN, BRETT R. GOLDSMITH AND PHILIP G. COLLINS*

Department of Physics and Astronomy, University of California at Irvine, Irvine, California 92697-4576, USA

*e-mail: collinsp@uci.edu

Published online: 6 November 2005; doi:10.1038/nmat1516

The prevailing conception of carbon nanotubes and particularly single-walled carbon nanotubes (SWNTs) continues to be one of perfectly crystalline wires. Here, we demonstrate a selective electrochemical method that labels point defects and makes them easily visible for quantitative analysis. High-quality SWNTs are confirmed to contain one defect per 4 μm on average, with a distribution weighted towards areas of SWNT curvature. Although this defect density compares favourably to high-quality, silicon single-crystals, the presence of a single defect can have tremendous electronic effects in one-dimensional conductors such as SWNTs. We demonstrate a one-to-one correspondence between chemically active point defects and sites of local electronic sensitivity in SWNT circuits, confirming the expectation that individual defects may be critical to understanding and controlling variability, noise and chemical sensitivity in SWNT electronic devices. By varying the SWNT synthesis technique, we further show that the defect spacing can be varied over orders of magnitude. The ability to detect and analyse point defects, especially at very low concentrations, indicates the promise of this technique for quantitative process analysis, especially in nanoelectronics development.

A decade ago, Ebbesen[1] declared that "Evidence is accumulating that carbon nanotubes are rarely as perfect as they were once thought to be". Nevertheless, each main advance in SWNT synthesis[2–6] reasserts the claim of defect-free materials, usually supported by macroscopic characterization such as Raman spectroscopy[7–9]. Such claims are difficult to substantiate or refute at the extremely low defect densities that affect device electronics, in part because of the experimental difficulty of directly imaging point defects. Atomic-resolution scanning tunnelling microscopy (STM) is a powerful technique for identifying SWNT defects[10–12], but is too slow and painstaking for statistically relevant material characterization and it cannot be performed on insulating gate oxides. Raman spectroscopy lacks the resolution to directly identify a single defect in otherwise pristine material[13]. As a result, current attempts to commercialize nanotube-based electronics such as logic, memory and chemical-sensor circuits are proceeding with little quantitative knowledge about the defect sites in SWNTs, even though such sites may disproportionately affect the chemical, mechanical and electronic properties of SWNTs and critically enable or disable certain desirable electronic properties[14].

Selective electrochemical deposition (SED) is one potential solution to efficiently and quantitatively measure defect densities in individual SWNTs and SWNT circuits, as well as to assist in the study of the electronic properties of defects. As demonstrated below, a sequence of electrochemical potentials applied to a SWNT can selectively nucleate metal deposition at the sites of highest chemical reactivity. As SWNT defect sites are more reactive than the pristine sp^2-bonded lattice, appropriate deposition potentials can decorate these sites with high selectivity. Research on highly oriented pyrolytic graphite (HOPG) has proven the general principle of SED[15–17]. Each step edge on a HOPG surface constitutes a line of chemical defects and by decorating these defects continuous millimetre-length nanowires may be grown using a variety of metals[17]. SWNTs are one-dimensional analogues of HOPG, sharing many of the same chemical and physical properties, so the cyclic voltammetry and electrochemical equilibria are nearly identical for the two materials[18].

To demonstrate and test SED on SWNT circuits, devices were fabricated using standard techniques[4] and then modified in a custom electrochemical cell. First, small-diameter SWNTs were

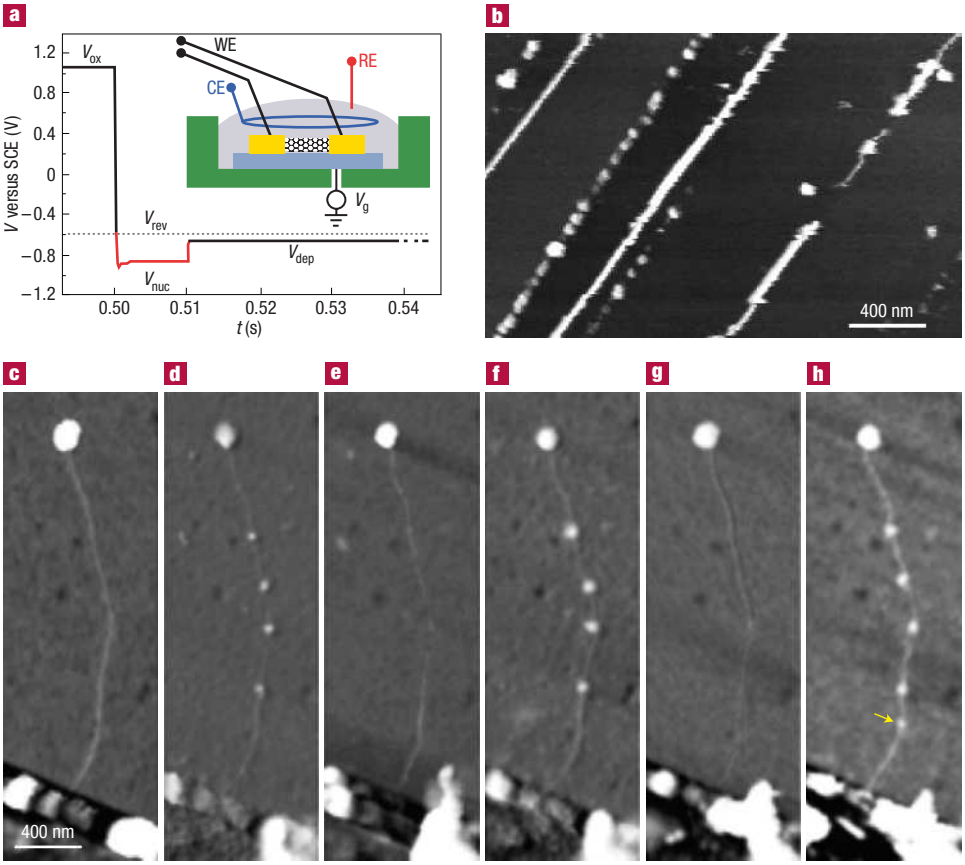

Figure 1 Selective nucleation at chemical defects on HOPG and SWNTs. a,**b**, A tri-potential electrochemical pulse (**a**) deposits metal almost continuously along the long, parallel step edges of freshly cleaved HOPG (**b**). The key portion of this pulse, highlighted in red in **a**, is a short overpotential during which selective nucleation occurs (*t* is time). The inset in **a** depicts the general electrochemical setup as described previously[20]. WE, working electrode; CE, counter electrode; RE, reference electrode. Virtually no deposition occurs on the HOPG terraces under appropriate conditions. **c**,**d**, Identical electrochemical potentials applied to a topographically clean SWNT circuit (**c**) decorate the SWNT's most chemically reactive sites (**d**). These images show a 2-μm segment of a 1.8-nm-diameter SWNT. The SWNT bridges a Au/Ti electrode (bottom) and a catalyst-impregnated alumina particle (top). Electrochemical growth for 10 s has deposited uniform nickel dots 14 nm in diameter. **e**–**h**, The deposits are easily removed, either electrochemically or by acid etching (**e**,**g**) and redeposition results in new deposits at identical positions (**f**,**h**). Acid etching was most effective at completely removing the metal dots and recovering a topographically clean nanotube, but this treatment can also create new reactive sites such as indicated by the arrow (**h**). The tri-potential pulse, on the other hand, has no effect on the number of positions. Repeated cycles of deposition and etching also roughen the Au electrodes. The scale bar in **c** also applies to **d**–**h**.

grown by chemical vapour deposition (CVD) of methane at 950 °C using alumina-supported iron nitrates[4] or iron Keggin molecules[19] as catalysts. The SWNTs were contacted at multiple positions by Au-coated Ti electrodes fabricated using optical lithography on thermally oxidized Si wafers. The completed devices were mounted in an electrochemical cell and modified with the aid of a platinum counter electrode and either a platinum or saturated calomel reference electrode (SCE). The measurement configuration reproduces previous work[20] and is schematically depicted in Fig. 1a. The SWNT and its connective lithography constituted the working electrode, as contacted by moveable probe tips coated with insulating photoresist. Wirebonding the devices with fine aluminium wire worked equally well owing to aluminium's native surface oxide, but this configuration proved much less versatile. The complete measurement cell integrated a fluid delivery system and a dry nitrogen environment to limit spurious oxidation of the electrolytes.

Figure 1 demonstrates SED results on freshly cleaved HOPG substrates and on SWNT circuits, as imaged in air by non-contact atomic force microscopy (AFM, JEOL JSPM-5200). For both samples, nickel metal was deposited for 60 s from a buffered electrolyte (1 mM $NiSO_4$ in 0.1 M Na_2SO_4 at pH 5.0) at a deposition potential $V_{dep} = -0.65$ V versus SCE. In Fig. 1b, uniform decoration of the HOPG step edges combined with nearly pristine step terraces indicate the high degree of selectivity that can be achieved and the high efficiency of defect site decoration. Using identical conditions, a few metal dots nucleate and grow on a SWNT (Fig. 1d), even though the initial microscopy of the SWNT is topologically smooth (Fig. 1c). Although a perfectly crystalline SWNT should behave like the inert HOPG terraces, particular sites on any given SWNT show the reactivity of the broken bonds at a HOPG step edge.

Extending the deposition time uniformly increases the size of the metal deposits without nucleating new sites. Alternatively, a positive electrochemical potential drives the anodic dissolution of nickel and can reduce the dot diameter, even completely removing the nickel from the SWNT. In this case, a topologically clean SWNT is recovered (Fig. 1e) and subsequent cycles of deposition repeatedly decorate the same SWNT positions. A typical test cycle of deposition, removal and redeposition is shown in Fig. 1c–h. Following each step in the cycle, the device was transferred out

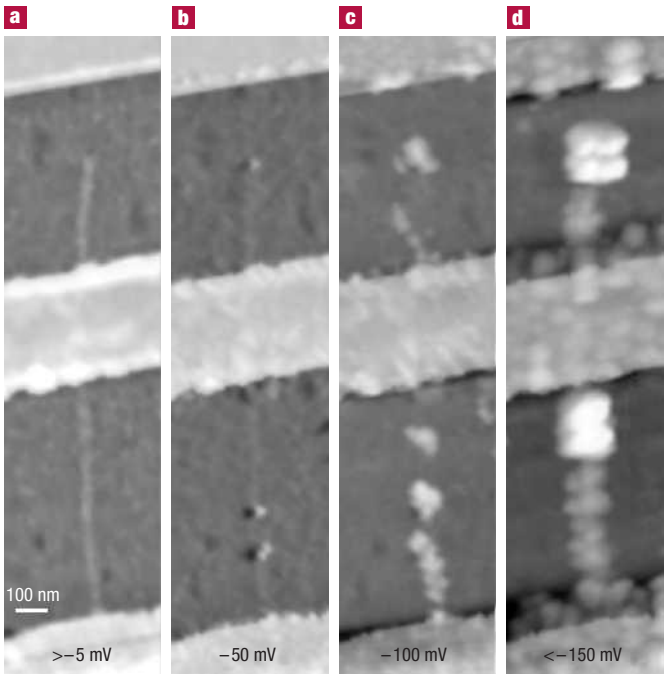

Figure 2 Selective versus non-selective growth can be controlled by the deposition potentials. Selective decoration of a SWNT occurs in a relatively narrow deposition window slightly negative of V_{rev}, the metal's reversible equilibrium potential. **a**–**d**, A series of depositions at progressively increasingly negative overpotentials $V_{dep}-V_{rev}$ results in no modification (**a**), selective deposition (**b**) and non-selective deposition (**c**,**d**). Overpotentials in the range of −10 to −50 mV give the best results, reliably and reversibly decorating the SWNT tip as well as two sidewall positions. Increasingly negative overpotentials increase the growth rate but also promote random nucleation. The interelectrode spacing in this image is 0.7 μm and the SWNT diameter is 1.6 nm. The scale bar in **a** also applies to **b**–**d**.

of the cell with a rigorous washing procedure in deionized water and then imaged in air by AFM. The metal removal step can be executed equally well by electrochemical stripping or by washing a device in dilute acid. The acid treatment, however, produces new nucleation sites on SWNTs at a low but measurable rate. One such new site is identified in Fig. 1h. On the basis of our experience of testing devices through many deposition cycles, we observe the creation of approximately one new site per micrometre of SWNT for each hour of total soak time in 12% HCl. Presumably, any combination of heating, ultrasonication and higher acid activity might lead to even higher production of nucleation sites, but this hypothesis remains to be tested. When acid removal is not used, the number and location of electrochemically labelled sites remains constant through dozens of cycles.

These results demonstrate that SED reliably identifies sites on SWNTs that have the enhanced reactivity of HOPG step edges. These sites are not mobile or random from cycle to cycle, so they are functionally equivalent to immobile chemical defects. The images also indicate that these sites are decorated with a very high efficiency. This efficiency is key to the use of SED for quantitative defect characterization and is a direct consequence of a specially tailored tri-potential pulse described below.

The deposition potential $V_{dep} = -0.65$ V used here is approximately 0.07 V more negative than the working electrode's reversible potential for Ni electrodeposition $V_{rev} = -0.58$ V versus SCE. This is a relatively small, negative overpotential, using the standard electrochemical definition of overpotential as the difference $V_{dep}-V_{rev}$. Deposition at a small overpotential ensures slow, kinetically limited deposition[16] of Ni at nucleated sites and simultaneously is insufficient to nucleate new deposition on the bare carbon surface. Nucleation is instead controlled by the potential profile preceding V_{dep}. As first described and implemented for HOPG[16], an oxidation pulse followed by a nucleation pulse can first chemically prepare the surface and then selectively nucleate metal growth in preparation for further deposition. The objective here is both to amplify defects that might otherwise fail to nucleate and also to suppress random nucleation on defect-free regions of SWNTs. Amplification is achieved by subjecting SWNTs to mild oxidation at $V_{ox} = +1.10$ V for 0.5–5 s. This oxidation does not affect the pristine sp^2 lattice, but at defects it will form carbonyls, ethers, hydroxyls and other oxygen-containing functionalities[21], all of which facilitate the nucleation of metal. Some oxidation-resistant functionalities may not be activated by this treatment, but we have not observed any increase in either the HOPG or SWNT site density for V_{ox} up to 1.5 V. Following the oxidation step, a nucleation pulse with amplitude $V_{nuc} = -0.85$ V and duration $\tau_{nuc} = 10$ ms initiates growth at these prepared sites. The height of V_{nuc} is optimized so that metal deposition may be nucleated with nearly 100% efficiency. At this relatively small overpotential, random nucleation on the pristine lattice proceeds slowly and can be limited quite effectively by a short τ_{nuc}. In our case, durations τ_{nuc} of 10–50 ms repeatedly decorated specific sites with virtually no random nucleation. A home-built bipotentiostat system controlled the potentials and durations of our tri-potential sequence, a portion of which is depicted in Fig. 1a.

An enabling factor for the selectivity of SED is the continuous electronic control one has over the electrochemical potentials. Chemically selective deposition occurs on SWNTs and HOPG step edges in a relatively narrow potential window. Figure 2 quantifies this effect for a SWNT circuit in which the end of the SWNT is in the field of view, guaranteeing the presence of at least one true chemical defect. For underpotentials $V_{dep} > V_{rev}$, repeated cycling never modified the SWNT measurably (Fig. 2a). Small overpotentials in the range of −20 to −50 mV clearly label the SWNT endpoint as well as two other chemically reactive sites (Fig. 2b). Making V_{dep} increasingly negative increases the decoration site density, but without the same site selectivity seen at lower overpotentials. Further lowering of V_{dep} can result in uniform coverage of the entire SWNT (Fig. 2d), which can be useful for the templated growth of metal nanowires as demonstrated in refs 22,23. The various depositions can be done in any order and a lack of history dependence limits the possible role the tri-potential pulse might play in producing new defects. To support this conclusion, Fig. 2 is presented chronologically backwards, with the overdeposition Fig. 2d performed first in time and the final resistance to deposition Fig. 2a performed last.

Many important differences exist between the nickel electrodeposits at preferred sites and the 'excess' deposits observed in Fig. 2c,d. First, the excess deposits tend to be smaller and more widely distributed in diameter. Second, the number of excess dots is random and increases with the deposition time or from one SED cycle to the next. Third, stripping all of the metal and starting anew on the same SWNT leads to a spatial redistribution of the excess deposition but not of the preferred sites. All of these observations implicate nucleation at random times during the duration of V_{dep} rather than during the nucleation pulse. One can confidently determine and maintain appropriate threshold deposition potentials to exclude this kind of random deposition and, as the SED process is reversible, we routinely run multiple SED cycles on each sample.

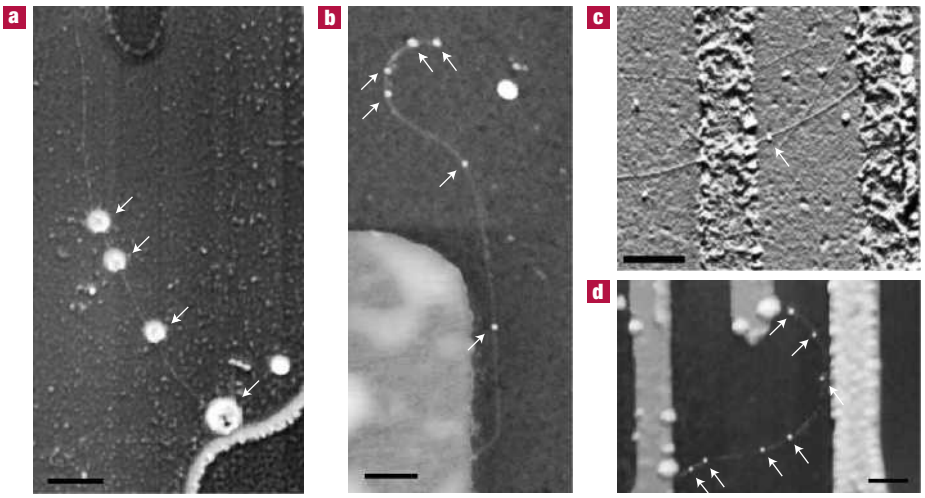

Figure 3 Variability in defect spacing. Decoration of many devices allows the determination of a mean defect density for a particular batch of CVD-grown SWNTs. Each SWNT shown here is grown simultaneously on a single wafer and then decorated by SED. Depositions tested for reproducibility using the procedure of Fig. 1 are marked by arrows. **a**,**b**, Some SWNTs extend well past their connecting electrodes, allowing the identification of long, defect-free regions and closely-spaced defects within the same SWNT. The bipolar distribution makes a simple average spacing somewhat misleading. **c**, The low defect density allows a majority of two-terminal devices to have zero or only one defect site when appropriate electrode separations are used. In this work, an electrode spacing of 0.7 μm led 10% of the devices to incorporate a single defect. **d**, Curved sections of SWNTs incorporate a higher density of defects and skew the overall average lower (**b**,**d**). The scale bar in each image is approximately 0.5 μm. The diameters of the depositions are approximately 200 nm in **a** and 15 nm in **b**–**d**.

A useful feature of the tri-potential sequence is that the final size of the metal deposits depends solely on the duration of the deposition potential V_{dep} and is therefore completely independent of the selectivity or efficiency of nucleation. Over the first few minutes of growth, the metal dots grow rapidly from a few nanometres up to 50–100 nm (see, for example, Fig. 3a). At this size, the dots can be readily identified by wide-field scanning electron microscopy, allowing large numbers of SWNT devices to be simultaneously assessed (in this work, however, AFM was used exclusively to avoid the deposition of coatings that might interfere with reversibility and reproducibility). By increasing the growth time to an hour or more, the dots even become visible to side-illuminated or dark-field optical microscopy.

Remarkably, this SED technique can magnify an atomic point defect to the extent that it becomes visible for counting by eye. Similar but non-reversible amplification techniques are necessary to quantify the low defect densities present in high-quality, Czochralski-grown Si crystals[24,25]. By comparison, Raman spectroscopy is unable to distinguish such sites individually, even with the aid of surface-enhanced resonant scattering. In fact, the complete absence of any disorder, or 'D-band', Raman spectral feature around the section of a SWNT known to contain a defect was shown in ref. 13. At higher defect densities, Raman spectroscopy is an invaluable tool for the characterization of bulk and individual SWNTs[26], but in the low-density limit relevant for electronic applications, far-field Raman fails to identify disorder. The strong D-band signal from SWNT ends[27] further complicates the identification of nearby defects as readily observed in Figs 1 and 2.

To demonstrate the further application of SED, a 4-inch wafer of devices was manually tested for SWNT defects. More than 200 SWNTs in circuits were tested for defects, a few of which are presented in Fig. 3. Although each individual device was defined by a source–drain distance of 0.7 μm, the total cumulative length of SWNTs tested exceeded 1.0 mm because many of the SWNTs extended a few micrometres beyond the source–drain region, just as in Fig. 1. As all of the SWNTs were grown and contacted under identical conditions, SED allows meaningful statistics to be derived on the material quality and device behaviour. Hundreds of defect sites were readily identified and a simple division of this total by the cumulative length gives a defect density of one per 4 μm (similar to estimates from transport measurements[28]). However, the distribution was notably non-uniform and somewhat bipolar, even though the decorated positions were in general randomly distributed. Many SWNTs showed sections 1–2 μm long without a single defect, whereas others had many defects clustered together as shown in Figs 1 and 3. The separation distance between consecutive defects on a single SWNT was measured to have a mean value of 0.36 μm, significantly shorter than the 4 μm average would imply. A large standard deviation $\sigma = 0.33$ μm is indicative of the wide variability in defect spacing. Finally, even though local topological effects at defect sites were not apparent, gradually curved SWNT segments definitely showed higher defect densities than straight segments, possibly indicating that small fluctuations in the CVD environment can directly influence the introduction of defects during growth. This effect is clearly shown in Fig. 3b,d.

To put these results into context, we compare the average defect density of one site per 4 μm to modern semiconductor technologies. This density corresponds to one site per 10^{12} atoms, comparable to high-quality Si crystals that typically have oxygen impurities of one per 10^{13} atoms and silicon vacancies or interstitials of one per 10^{12} atoms[24,25]. A continuing technical difficulty in semiconductor processing is the identification and counting of crystal defects, which individually are too small for most spectroscopies. The fact that SWNT conductors are hollow surfaces enables the SED technique to be used for accurate defect counting. A second consideration is that low-density SWNT networks may be useful thin-film conductors or transistors[29]. At a typical surface density of a few SWNTs per μm^2, the areal defect density is a mere 10^9 sites per cm^2. This is a remarkably low density for thin-film active electronics, particularly compared with polymers, organics or other flexible alternatives to conventional Si.

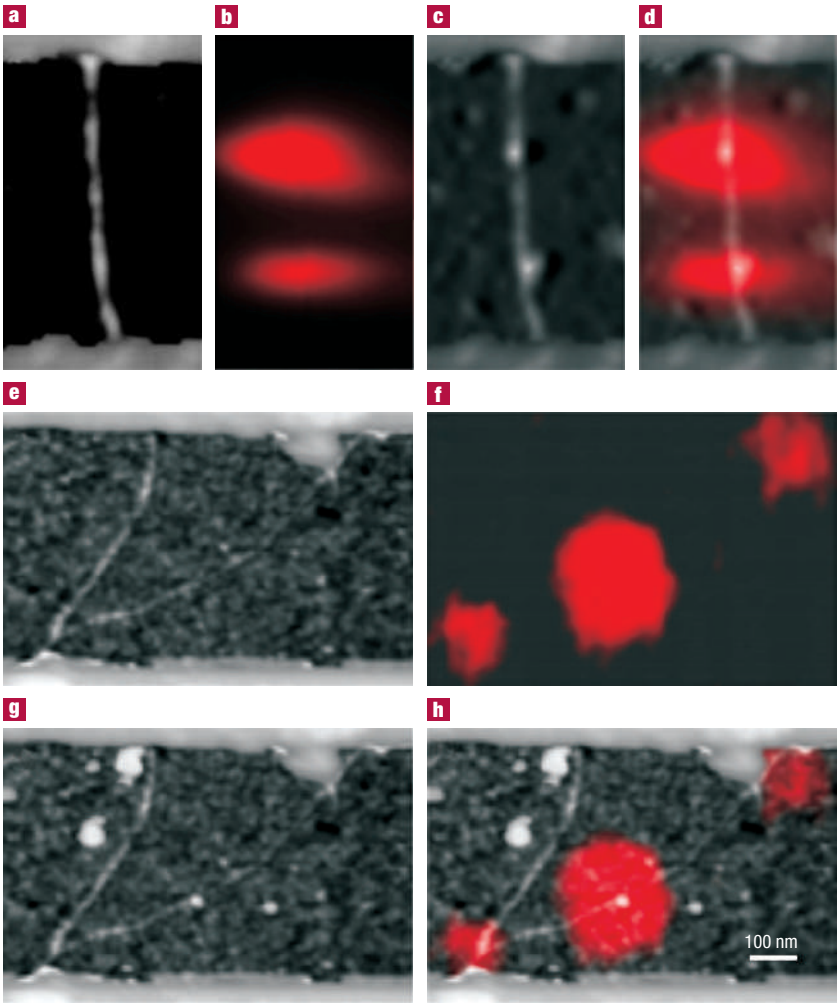

Figure 4 Correspondence between local electronic resistance and sites of enhanced chemical reactivity. Images of topography, a.c. SGM (red overlay) and selective deposition for two different SWNT circuits. **a**,**b**, In the first device, a single, clean SWNT (**a**) shows two areas of large, local gate dependence (**b**). **c**,**d**, Subsequent SED on this device produces two metal dots (**c**) having a one-to-one spatial correspondence with the electronically active sites, as demonstrated by building up a composite image (**d**). **e**, In a second device, two SWNTs are found. **f**, The longer SWNT shows gate-sensitive Schottky barriers at both ends, in addition to a gate-sensitive spot near its midpoint. **g**,**h**, Using SED, a chemically active defect is found (**g**) at the same position as the electronic sensitivity (**h**). Thus we infer that this SWNT has a semiconducting band structure and a single defect. The shorter SWNT in this image shows no electronic sensitivities or defects and can be interpreted as a defect-free, metallic SWNT. The scale bar in **h** also applies to **a**–**g**.

We have explored the possibility that variations in synthesis parameters might significantly change this SWNT defect density. SWNTs grown *ex situ* by arc vaporization, suspended in solvent and deposited onto a wafer surface have shown deposition densities exceeding one dot per 100 nm. Alternatively, run-to-run variations in CVD growth parameters have produced SWNTs with average defect-to-defect separations much greater than 1 μm. In our best results so far, only two defect sites have been identified in approximately 200 μm of CVD-grown SWNTs grown in the Burke research group at UCI[30]. Thus, SED provides a direct quantitative method to distinguish between nominally identical CVD runs, and it may become a useful quality and process control technique for reproducible SWNT electronics.

To emphasize this point, consider the prototypical SWNT transistor device[31]. Previous researchers have attributed transistor switching to conventional band shifts, Schottky barriers[32] and also to resonant scattering by defects[33]. To identify and distinguish between these mechanisms, scanning gate microscopy (SGM) has been used successfully[33–35]. In SGM, different sections of a SWNT are gated independently with 10-nm resolution in order to determine where the device's field sensitivity is localized. We use an a.c. variant[36] of SGM that, when performed in high vacuum, enhances signal-to-noise and minimizes hysteretic substrate effects.

Figure 4 shows two SWNT-based circuits characterized by both SED and SGM. Both devices show typical, p-type, gate-dependent conductivities $G(V_g)$. The device in Fig. 4a is composed of a single SWNT and the entire effect of gating is found to be localized at two positions along the SWNT body (Fig. 4b). These spots constitute electronic defects in the sense that they disproportionately contribute to the device's two-terminal transconductance dI/dV_g. Otherwise, one may conclude that this particular SWNT has a metallic band structure because it does not show gate-sensitive Schottky barriers at the Ti electrode interfaces. Subsequent SED testing demonstrates the growth of two metal dots on the SWNT (Fig. 4c). Owing to the interference of the conductive electrolyte, SGM and SED may not be done simultaneously, but a

composite image of the two experiments shows a perfect one-to-one correspondence between the 'electronic' defect sites and the chemical sites (Fig. 4d).

Similar results are shown on a second device having two SWNTs (Fig. 4e–h). Here, interfacial Schottky barriers help to clearly identify one SWNT as a semiconductor (Fig. 4f). In addition to local sensitivity at its interfaces, this SWNT shows an even greater gate dependence at a single site midway along its length, and SED testing grows a single metal particle at this site (Fig. 4g). Moreover, no deposition is observed on the rest of the device (either at the Schottky barriers or on the metallic, gate-insensitive SWNT), confirming the hypothesis that SGM sensitivity on a SWNT body directly corresponds to local chemical reactivity.

Both samples shown in Fig. 4 show transistor-like behaviour due, at least in part, to the presence of locally sensitive sites. Approximately 10% of our transistor devices show such sites when characterized by SGM, but SGM is too time-consuming to be used for regular batch characterization. The SED process, on the other hand, quickly identifies the same features with better spatial resolution; SWNT circuits with zero, one or more defects may be easily identified, even at the wafer scale, to complement electrical characterization. The examples confirm the electronic importance of chemical defects, even at very low concentrations, and suggest that the D-band Raman signal may be a useful but insufficient indicator of SWNT quality when it comes to electronic applications.

We have not yet determined whether the electrical characteristics of the devices are permanently or reversibly changed by the chemical modifications of SED, and this remains a topic for future work. One would hope to compare the electronic effects of this chemical modification with theoretical models[14] and also couple the SED technique to broader classes of functionalization[37] that might modify the electronic behaviour in controlled and useful directions.

Finally, SED is chemically selective but not sufficiently so to distinguish the chemical nature of the reactive site being detected. A rotated bond (Stone–Wales defect), a substitutional dopant, a broken bond passivated by further chemical groups or a mechanical strain or kink are all candidate defect mechanisms in SWNTs. Extrinsic trapped charges in the underlying substrate or adsorbed contaminant ions may also result in localized chemical reactivity (as well as electronic effects), and these are lumped together with true sidewall defects by the SED technique. Further spectroscopies, coupled with process variations, might be able to distinguish between some of these cases. Raman, for example, is able to confirm the presence of a defect in the special case where that defect changes the chirality of the SWNT[13,38]. From a purely practical perspective, all of these mechanisms are functionally equivalent. Both electronically and chemically, these defect sites and their SED identification may help clarify outstanding issues of variability, noise and reliability in SWNT electronics.

Received 23 May 2005; accepted 15 September 2005; published 6 November 2005.

References

1. Ebbesen, T. W. & Takada, T. Topological and sp3 defect structures in nanotubes. *Carbon* **33,** 973–978 (1995).
2. Thess, A. *et al.* Crystalline ropes of metallic carbon nanotubes. *Science* **273,** 483–487 (1996).
3. Cassell, A. M., Raymakers, J. A., Kong, J. & Dai, H. J. Large scale CVD synthesis of single-walled carbon nanotubes. *J. Phys. Chem. B* **103,** 6484–6492 (1999).
4. Kong, J., Soh, H. T., Cassell, A. M., Quate, C. F. & Dai, H. J. Synthesis of individual single-walled carbon nanotubes on patterned silicon wafers. *Nature* **395,** 878–881 (1998).
5. Nikolaev, P. *et al.* Gas-phase catalytic growth of single-walled carbon nanotubes from carbon monoxide. *Chem. Phys. Lett.* **313,** 91–97 (1999).
6. Hata, K. *et al.* Water-assisted highly efficient synthesis of impurity-free single-walled carbon nanotubes. *Science* **306,** 1362–1364 (2004).
7. Bom, D. *et al.* Thermogravimetric analysis of the oxidation of multiwalled carbon nanotubes: Evidence for the role of defect sites in carbon nanotube chemistry. *Nano Lett.* **2,** 615–619 (2002).
8. Hamon, M. A. *et al.* End-group and defect analysis of soluble single-walled carbon nanotubes. *Chem. Phys. Lett.* **347,** 8–12 (2001).
9. Dillon, A. C. *et al.* Systematic inclusion of defects in pure carbon single-wall nanotubes and their effect on the Raman D-band. *Chem. Phys. Lett.* **401,** 522–528 (2005).
10. Clauss, W. *et al.* Electron backscattering on single-wall carbon nanotubes observed by scanning tunneling microscopy. *Europhys. Lett.* **47,** 601–607 (1999).
11. Kim, H. *et al.* Direct observation of localized defect states in semiconductor nanotube junctions. *Phys. Rev. Lett.* **90,** 216107 (2003).
12. Ishigami, M. *et al.* Identifying defects in nanoscale materials. *Phys. Rev. Lett.* **93,** 196803 (2004).
13. Doorn, S. K. *et al.* Raman spectroscopy and imaging of ultralong carbon nanotubes. *J. Phys. Chem. B* **109,** 3751–3758 (2005).
14. Louie, S. G. in *Carbon Nanotubes* 113–145 (Springer, Berlin, 2001).
15. Zach, M. P., Ng, K. H. & Penner, R. M. Molybdenum nanowires by electrodeposition. *Science* **290,** 2120–2123 (2000).
16. Penner, R. M. Mesoscopic metal particles and wires by electrodeposition. *J. Phys. Chem. B* **106,** 3339–3353 (2002).
17. Walter, E. C. *et al.* Metal nanowire arrays by electrodeposition. *Chem. Phys. Chem.* **4,** 131–138 (2003).
18. Banks, C. E., Davies, T. J., Wildgoose, G. G. & Compton, R. G. Electrocatalysis at graphite and carbon nanotube modified electrodes: edge-plane sites and tube ends are the reactive sites. *Chem. Commun.* 829–841 (2005).
19. An, L., Owens, J. M., McNeil, L. E. & Liu, J. Synthesis of nearly uniform single-walled carbon nanotubes using identical metal-containing molecular nanoclusters as catalysts. *J. Am. Chem. Soc.* **124,** 13688–13689 (2002).
20. Kruger, M., Buitelaar, M. R., Nussbaumer, T., Schonenberger, C. & Forro, L. Electrochemical carbon nanotube field-effect transistor. *Appl. Phys. Lett.* **78,** 1291–1293 (2001).
21. Chen, J. *et al.* Solution properties of single-walled carbon nanotubes. *Science* **282,** 95–98 (1998).
22. Braun, E., Eichen, Y., Sivan, U. & Ben-Yoseph, G. DNA-templated assembly and electrode attachment of a conducting silver wire. *Nature* **391,** 775–778 (1998).
23. Heller, I. *et al.* Individual single-walled carbon nanotubes as nanoelectrodes for electrochemistry. *Nano Lett.* **5,** 137–142 (2005).
24. Kissinger, G., Gräf, D., Lambert, U., Grabolla, T. & Richter, H. Key influence of the thermal history on process-induced defects in Czochralski silicon wafers. *Semicond. Sci. Technol.* **12,** 933–937 (1997).
25. Xi, Z., Chen, J., Yang, D., Lawerenz, A. & Moeller, H. J. Copper precipitation in large-diameter Czochralski silicon. *J. Appl. Phys.* **97,** 094909 (2005).
26. Dresselhaus, M. S. *et al.* Science and applications of single-nanotube Raman spectroscopy. *J. Nanosci. Nanotechnol.* **3,** 19–37 (2003).
27. Pimenta, M. A. *et al.* Diameter dependence of the Raman D-band in isolated single-wall carbon nanotubes. *Phys. Rev. B* **64,** 041401 (2001).
28. Mann, D., Javey, A., Kong, J., Wang, Q. & Dai, H. J. Ballistic transport in metallic nanotubes with reliable Pd ohmic contacts. *Nano Lett.* **3,** 1541–1544 (2003).
29. Bradley, K., Gabriel, J. C. P. & Gruner, G. Flexible nanotube electronics. *Nano Lett.* **3,** 1353–1355 (2003).
30. Li, S. D., Yu, Z., Rutherglen, C. & Burke, P. J. Electrical properties of 0.4 cm long single-walled carbon nanotubes. *Nano Lett.* **4,** 2003–2007 (2004).
31. Yao, Z., Dekker, C. & Avouris, P. in *Carbon Nanotubes* 147–171 (Springer, Berlin, 2001).
32. Heinze, S. *et al.* Carbon nanotubes as Schottky barrier transistors. *Phys. Rev. Lett.* **89,** 106801 (2002).
33. Bockrath, M. *et al.* Resonant electron scattering by defects in single-walled carbon nanotubes. *Science* **291,** 283–285 (2001).
34. Bachtold, A. *et al.* Scanned probe microscopy of electronic transport in carbon nanotubes. *Phys. Rev. Lett.* **84,** 6082–6085 (2000).
35. Tans, S. J. & Dekker, C. Molecular transistors — potential modulations along carbon nanotubes. *Nature* **404,** 834–835 (2000).
36. Freitag, M., Johnson, A. T., Kalinin, S. V. & Bonnell, D. A. Role of single defects in electronic transport through carbon nanotube field-effect transistors. *Phys. Rev. Lett.* **89,** 216801 (2002).
37. Banerjee, S., Hemraj-Benny, T. & Wong, S. S. Covalent surface chemistry of single-walled carbon nanotubes. *Adv. Mater.* **17,** 17–29 (2005).
38. Duesberg, G. S. *et al.* Experimental observation of individual single-wall nanotube species by Raman microscopy. *Chem. Phys. Lett.* **310,** 8–14 (1999).

Acknowledgements

We thank Nanomix, R. Haddon, and P. Burke for supplying various types of SWNT for this study, N. Emmott for experimental assistance and R. Penner for sharing his expertise with HOPG. Partially funded by NSF 0404057 and the ACS PRF-39672-G5M.
Correspondence and requests for materials should be addressed to P.G.C.

Competing financial interests

The authors declare that they have no competing financial interests.